Differential volume regulation and calcium signaling in two ciliary body cell types is subserved by TRPV4 channels

Andrew O. Jo[a], Monika Lakk[a], Amber M. Frye[a], Tam T. T. Phuong[a], Sarah N. Redmon[a], Robin Roberts[b], Bruce A. Berkowitz[b,c], Oleg Yarishkin[a], and David Križaj[a,d,e,f,1]

[a]Department of Ophthalmology & Visual Sciences, University of Utah School of Medicine, Salt Lake City, UT 84132; [b]Department of Anatomy and Cell Biology, Wayne State University, Detroit, MI 48202; [c]Department of Ophthalmology, Wayne State University, Detroit, MI 48202; [d]Center for Translational Medicine, Moran Eye Institute, University of Utah, Salt Lake City, UT 84132; [e]Department of Neurobiology & Anatomy, University of Utah, Salt Lake City, UT 84132; and [f]Department of Bioengineering, University of Utah, Salt Lake City, UT 84132

Edited by King-Wai Yau, Johns Hopkins University School of Medicine, Baltimore, MD, and approved February 23, 2016 (received for review August 11, 2015)

Fluid secretion by the ciliary body plays a critical and irreplaceable function in vertebrate vision by providing nutritive support to the cornea and lens, and by maintaining intraocular pressure. Here, we identify TRPV4 (transient receptor potential vanilloid isoform 4) channels as key osmosensors in nonpigmented epithelial (NPE) cells of the mouse ciliary body. Hypotonic swelling and the selective agonist GSK1016790A (EC_{50} ~33 nM) induced sustained transmembrane cation currents and cytosolic $[Ca^{2+}]_i$ elevations in dissociated and intact NPE cells. Swelling had no effect on $[Ca^{2+}]_i$ levels in pigment epithelial (PE) cells, whereas depolarization evoked $[Ca^{2+}]_i$ elevations in both NPE and PE cells. Swelling-evoked $[Ca^{2+}]_i$ signals were inhibited by the TRPV4 antagonist HC067047 (IC_{50} ~0.9 μM) and were absent in *Trpv4*$^{-/-}$ NPE. In NPE, but not PE, swelling-induced $[Ca^{2+}]_i$ signals required phospholipase A2 activation. TRPV4 localization to NPE was confirmed with immunolocalization and excitation mapping approaches, whereas in vivo MRI analysis confirmed TRPV4-mediated signals in the intact mouse ciliary body. *Trpv2* and *Trpv4* were the most abundant vanilloid transcripts in CB. Overall, our results support a model whereby TRPV4 differentially regulates cell volume, lipid, and calcium signals in NPE and PE cell types and therefore represents a potential target for antiglaucoma medications.

TRPV4 | ciliary body | intraocular pressure | aqueous humor | glaucoma

Formation of aqueous humor in the vertebrate eye takes place within the ciliary body (CB), a highly folded tissue consisting of pigmented epithelial (PE) cells, nonpigmented epithelial (NPE) cells, and the ciliary muscle (1, 2). Together, PE cells, which face the vascularized stroma and represent a forward continuation of the retinal pigment epithelium (RPE), and NPE cells, which face the posterior chamber (lumen) of the eye and extend the neuronal retina, form the blood–aqueous barrier and regulate the production and secretion of aqueous humor. The aqueous fluid supplies nutrients and oxygen to nonvascularized tissues (lens, cornea, and trabecular meshwork) and is ultimately drained through the ciliary muscle and the trabecular meshwork in the anterior chamber of the eye. Aqueous secretion is subserved by the unidirectional transport of ions and water through gap junctions between PE cells and NPE cells (3, 4) and is driven by the osmotic gradient generated by Na^+/K^+ exchange across basolateral NPE membranes (2–5). Despite the critical dependence of aqueous humor secretion on osmotic pressure (1, 4, 6), the molecular mechanism through which NPE and PE cells sense and regulate changes in volume is not well understood.

In addition to osmotic shifts, CB cells experience mechanical forces associated with mean and time-varying aspects of intraocular pressure (IOP), a phenomenon that reflects balanced regulation of fluid secretion from NPE cells and its drainage from the anterior eye. Excessive IOP elevations represent the primary, and major, risk factor for contracting glaucoma (6, 7), an optic neuropathy that represents the second leading cause of blindness in the world. Therefore, aqueous secretion is often targeted by antiglaucoma medications that include β-adrenergic receptor antagonists, carbonic anhydrase inhibitors, α_2-adrenergic agonists, and muscarinic cholinergic agonists (7). A key question, however, is whether CB cells themselves are able to sense force mediated by membrane stretch induced by hydrostatic pressure or swelling, and what such mechanisms might be.

Here, we identify a key osmosensor in CB as transient receptor potential channel vanilloid isoform 4 (TRPV4), a polymodal nonselective cation-permeable channel that has been implicated in mechanotransduction (8, 9) as well as regulation of paracellular permeability in multiple epithelial tissues (10–15). Intriguingly, we found that TRPV4 is selectively distributed across CB by being confined to the NPE and excluded from PE cells. We characterized the functional role of TRPV4 as the predominant NPE swelling sensor and determined its contribution to swelling-dependent intracellular second messenger signaling mediated through calcium ions and long-chain, polyunsaturated lipids associated with the phospholipase A2 (PLA2) pathway. By elucidating the molecular mechanisms that underlie differential volume regulation in the two CB constituent cell types, and characterizing their susceptibility to lipid messenger modulation, our findings may provide new insight into the mechanism of aqueous fluid secretion and IOP modulation. A preliminary account of this work has been recently given (16).

Results

TRPV4 Immunolocalization Within the CB. We sought to determine the identity of the osmotransducer that links hypotonic stimuli to

Significance

The secretion of aqueous humor from the ciliary body is regulated by osmotic gradients, yet the mechanism through which these cells sense these gradients is still under debate. We have identified the calcium-permeable transient receptor potential vanilloid isoform 4 (TRPV4) ion channel as critical for translating hypotonic stimuli into intracellular signals and linked the activation of this channel to a known proinflammatory lipid signaling pathway. The channel was confined to nonpigmented cells that secrete aqueous fluid and regulate intraocular pressure. Thus, activation of TRPV4 may contribute to vision through metabolic support of anterior eye tissues and regulation of osmotic and tensile homeostasis within the eye.

Author contributions: A.O.J. and D.K. designed research; A.O.J., M.L., A.M.F., T.T.T.P., S.N.R., R.R., B.A.B., and O.Y. performed research; A.O.J., T.T.T.P., S.N.R., B.A.B., O.Y., and D.K. analyzed data; and D.K. wrote the paper.

The authors declare no conflict of interest.

This article is a PNAS Direct Submission.

[1]To whom correspondence should be addressed. Email: david.krizaj@hsc.utah.edu.

This article contains supporting information online at www.pnas.org/lookup/suppl/doi:10.1073/pnas.1515895113/-/DCSupplemental.

Ca^{2+} homeostasis in CB cells by focusing on TRPV4, a nonselective cation channel that was originally identified by its sensitivity to hypotonic challenge (8, 17) but was also recently suggested to regulate melatonin release from the CB (18). Immunocytochemistry with a validated antibody (19, 20), showed clear TRPV4 immunoreactivity (ir) across the mouse CB. The fluorescent signal was predominantly concentrated in the ciliary processes of the pars plicata (arrows in Fig. 1*A*, *iv*), whereas stroma showed minimal immunoreactivity (arrowheads in Fig. 1*A*, *iv*). Staining was also observed in the corneal epithelium that anchors the CB (arrowhead in Fig. 1*A*, *ii*). The specificity of the signals was confirmed by concomitant staining of *Trpv4*$^{-/-}$ tissue, which showed markedly lower fluorescence compared with the WT CB and by labeling CB tissue from nonpigmented mice (Fig. S1).

Because vanilloid TRP isoforms show a predilection toward heteromerization (21, 22), we evaluated the overall expression pattern of *Trpv4* and cognate vanilloid mRNAs in the mouse CB tissue. Primers targeting TRP isoforms (Table S1) showed strong expression for *Trpv2* and *Trpv4* transcripts in every sample ($n = 3$). Messenger RNAs produced by *Trpv1*, *Trpv3*, and *Trpv6* genes were also detected (Fig. S2), but their expression levels were markedly lower compared with isoforms 2 and 4. Down-regulation of *Trpv1* and *Trpv3*, but not *Trpv2,* gene expression in *Trpv4*$^{-/-}$ CB suggests that, as observed recently in the retina (23), TRPV4 activation might be linked to the transcription apparatus.

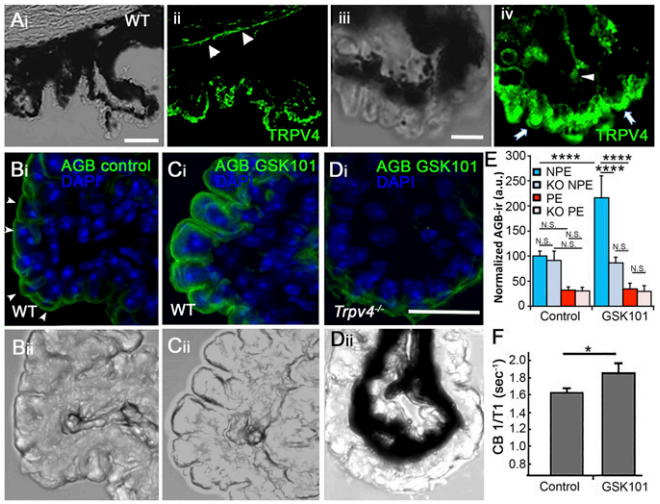

Fig. 1. Localization and functional expression of TRPV4 in the mouse CB. (*A*, *i* and *ii*) Vertical cryosections of WT mouse retinas immunolabeled for TRPV4 show preferential localization to the basolateral layer corresponding to NPE, with additional signals in the limbal corneal epithelium (arrowheads). (*i*) Transmitted image of the CB and the supporting cornea; (*ii*) TRPV4 immunoreactivity. (Scale bar, 100 μm.) (*iii* and *iv*) Close-up of the CB epithelium, showing TRPV4-ir in putative NPE cells (arrows). Modest immunofluorescence is detected in the putative stromal area (arrowhead). (Scale bar, 20 μm.) (*B–E*) Excitation mapping shows TRPV4-evoked cation influx into CB ex vivo. CBs were fixed, stained with an anti-AGB antibody (FITC), and counterstained with DAPI (blue). ROIs of equal size were placed around DAPI-positive cells in the NPE layer and PE layer, respectively. (*B, i* and *ii*) Transmitted + fluorescence image of isolated unstimulated (PBS-treated) nonpigmented CB tissue. (*C, i* and *ii*) Transmitted + fluorescence image of nonpigmented CB tissue stimulated with GSK101 (100 nM) and tested for AGB-ir + DAPI. (*D, i* and *ii*) Transmitted + fluorescence image of *Trpv4*$^{-/-}$ CB tissue stimulated with GSK101 simultaneously with preparations in *B* and *C*. (Scale bar, 20 μm.) (*E*) Quantification of fluorescence from GSK101-treated vs. PBS-treated WT and KO sections. $P < 0.005$. (*F*) In vivo CB signal evaluated using MEMRI. Quantification of average CB 1/T1 from vehicle ($n = 5$) and GSK101-treated (100 μM; $n = 5$) eyes. Values are presented as means ± SEM; *$P = 0.02$, ***$P < 0.005$, ****$P < 0.0001$.

Functional TRPV4 Expression in CB in Vivo and ex Vivo. To investigate functional TRPV4 expression at higher spatial resolution, we performed excitation mapping in intact CB sheets from WT and KO tissue. To eliminate the potentially confounding fluorescence screening by the pigment, the WT experiments were additionally performed in isolated from nonpigmented [*B6.Cg-Tg*(*Thy1-YFP*)*HJrs*/*J*] mouse eyes. Tissue was perfused with AGB^+, an immunogenic cation that has been used previously to mark activity-dependent cation permeability in vertebrate tissues, including the retina (20, 24), and double-labeled for DAPI to localize NPE vs. PE nuclei. The anti-AGB antibody showed a modest degree of ir at the basolateral membrane in unstimulated cells preincubated with the immunogen (arrowheads in Fig. 1*B*, *i*), suggesting unstimulated NPE experiences steady-state cation influx. Despite the steady-state AGB^+ signal in the basolateral NPE (Fig. 1*B*), comparison of fluorescence averaged across regions of interest (ROIs) positioned over NPE vs. PE layers showed them not to be significantly different (Fig. 1*E*). The selective agonist GSK1016790A (GSK101) (100 nM) profoundly enhanced AGB-ir at the basolateral edge of the NPE layer (Fig. 1 *C*, *i* and *E*), which expresses the highest density of TRPV4 channels (Fig. 1*A* and Fig. S1). The normalized AGB-ir in WT CB was 2.16 ± 0.34-fold higher in GSK101-exposed NPE cells compared with vehicle-treated controls ($P < 0.0001$; $n = 3$). The small (and nonsignificant; $P > 0.05$) increase in ir observed in the PE layer may be attributed to cation influx through gap junctions between the two epithelial layers and/or potential spillover of fluorescence from the NPE layer. AGB-ir in *Trpv4*$^{-/-}$ tissue (from pigmented animals) did not change following exposure to the TRPV4 agonist (Fig. 1*D*). Rather, the steady-state cation entry in GSK-treated and unstimulated CB KO cells was similar to signals observed in unstimulated WT cells (Fig. 1 *B–E*). These data demonstrate that functional TRPV4 signaling is mainly confined to the NPE layer with negligible cation influx into the PE layer or stroma. Interestingly, these data show that the basolateral NPE membrane supports steady-state, non-TRPV4-mediated cation influx that is counterbalanced by plasmalemmal clearance mechanisms that may include high-affinity calcium ATPases (PMCAs; Fig. S1*D*).

We took advantage of manganese-enhanced MRI (MEMRI) to evaluate the functional consequence of TRPV4 activation in the intact mouse eye. MEMRI, based on the activity-dependent Mn^{2+} influx as a contrast agent that readily permeates cation channels but is much more slowly removed through intracellular clearance mechanisms, represents the imaging modality of choice for noninvasively mapping ion influx into ocular cells in vivo (25–28). In vehicle-treated eyes, systemic (i.p.) injection of $MnCl_2$ resulted in a 51% increase over baseline CB 1/T1 values. Intravitreal injection of the GSK101 evoked an 86% increase in the CB over baseline that was statistically significant ($P < 0.05$) compared with eyes injected with the vehicle (PBS) (Fig. 1*F* and Fig. S3). These data are consistent with functional TRPV4 signals in the mouse CB.

Swelling Triggers TRPV4-Mediated $[Ca^{2+}]_i$ Increase in NPE, but Not PE, Cells. Although osmotic gradients are likely to play a key role in fluid ultrafiltration and aqueous secretion in the CB (2, 4), it is not yet known how CB cells sense the swelling impelled by hypotonic environments. Fig. 2 shows that the volume of both CB cell types is highly sensitive to a decrease in extracellular tonicity. A 37% decrease in tonicity at constant ionic strength, achieved by switching to hypotonic stimulation (HTS; 190 mOsm) from isotonic saline (300 mOsm), reversibly decreased fluorescence intensity in dissociated PE and NPE cells (Fig. 2 *A–C*), indicating an increase in cell volume. It was immediately apparent that NPE cells exhibit a greater tendency to swell compared with PE (Fig. 2*A*). Furthermore, in contrast to PE cells, fluorescent signals in NPE cells gradually recovered in the continued presence of HTS, indicative of regulatory volume decrease (RVD). Following

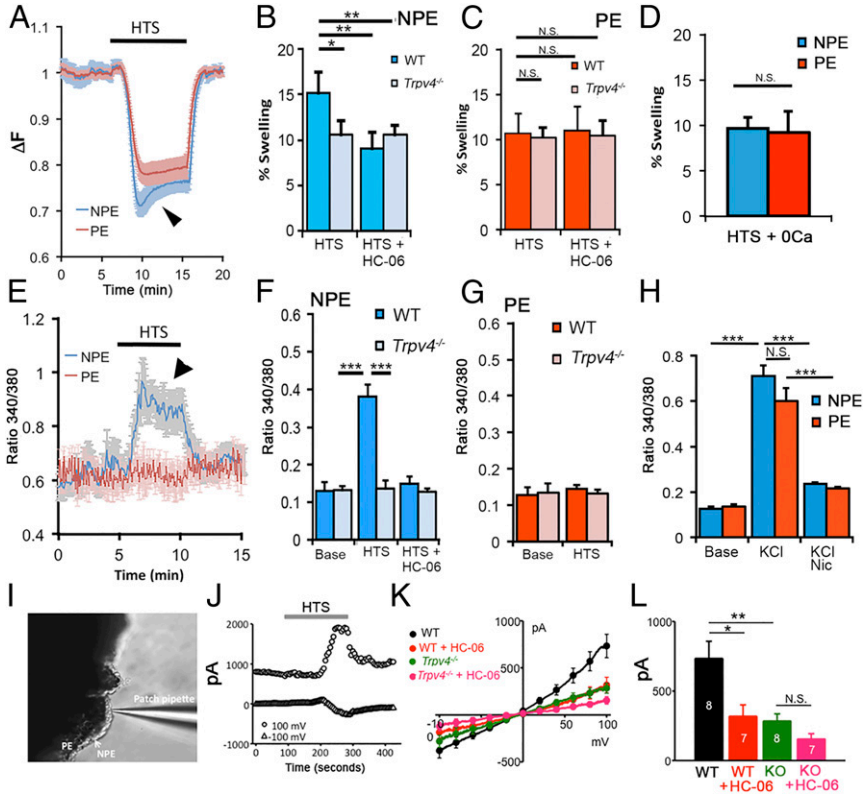

Fig. 2. Hypotonic challenge (190 mOsm) differentially regulates cell swelling and calcium homeostasis in dissociated NPE and PE cells. (*A*) Cell volume changes in concomitantly recorded NPE (blue) and PE (red) cells. The 340/380 Fura-2 ratio ΔF, adjusted to yield calcium-insensitive fluorescence, shows dose-dependent decreases as cell volume increases in the presence of hypotonic saline. Both volume increase and RVD (arrowhead) are more pronounced in NPE cells. (*B*) Percent swelling in NPE cells. WT cells (dark blue) swell more compared with *Trpv4*$^{-/-}$ cells (light blue); the TRPV4 antagonist HC-06 (1 μM) suppresses volume increase in WT ($n = 33$) but not KO cells ($n = 29$). (*C*) WT PE cells (dark red; $n = 30$) and *Trpv4*$^{-/-}$ cells (light red; $n = 31$). Percent swelling is unaffected by the loss of the *Trpv4* gene or TRPV4 antagonism. (*D*) NPE and PE cells swell by comparable amounts in the absence of extracellular Ca^{2+} ($n = 23$ and 27, respectively). (*E*–*G*) HTS elevates $[Ca^{2+}]_i$ in NPE ($n = 57$), but not PE ($n = 42$), cells. (*F*) HTS-evoked $[Ca^{2+}]_i$ signals are antagonized by HC-06 and absent in *Trpv4*$^{-/-}$ cells. (*G*) $[Ca^{2+}]_i$ levels in WT ($n = 46$) and KO ($n = 53$) PE cells are unaffected by HTS. (*H*) Thirty millimolar KCl. Depolarization evokes comparable $[Ca^{2+}]_i$ elevations in NPE (blue; $n = 23$) and PE (red, $n = 21$) cells. High KCl-induced signals were antagonized by the L-type channel blocker nicardipine. (*I*–*L*) Whole-cell patch clamp experiments. Hypotonicity activates TRPV4-mediated currents in NPE cells. (*I*) Experimental configuration with NPE recording in ex vivo CB tissue. (*J*) Representative time course of the whole-cell current in a NPE cell at the holding potentials of −100 mV and 100 mV. I-V curves taken immediately before the application of HTS (baseline) were subtracted from preceding and following traces. (*K*) Averaged current–voltage relationship curves of HTS-induced transmembrane currents in untreated control, *Trpv4*$^{-/-}$, and HC-06–treated NPE cells. The antagonist (5 μM) was administered at least 10 min before applying HTS. HTS-induced currents were calculated by subtracting I-V curves taken before the application of HTS from the peak response. (*L*) Cumulative data for GSK101-induced current amplitudes at +100 mV. The numbers in bars indicate the number of cells studied per each condition. Results are represented as mean ± SEM; *$P < 0.05$, **$P < 0.01$, ***$P < 0.005$.

termination of the hypotonic challenge, both NPE and PE cells rapidly recovered the initial volume.

To test whether HTS-induced swelling in CB cells is facilitated by TRPV4 activation, we exposed them to HTS in the presence of the selective antagonist HC067047 (HC-06). As illustrated in Fig. 2 *B* and *C*, HC-06 significantly suppressed the extent of HTS-induced increase in NPE cell volume but had little effect on swelling of (melanin-containing) PE cells. Consistent with this observation, the extent of cell swelling was inhibited in NPE cells isolated from *Trpv4*$^{-/-}$ tissues, whereas *Trpv4*$^{-/-}$ PE cells exhibited no differences from controls (Fig. 2 *B* and *C*). These findings suggest that TRPV4 channels differentially regulate swelling within the CB.

Given that TRPV4 channels are permeable to Ca^{2+} (P_{Ca}/P_{Na} ~6) (8, 9, 11), which regulates numerous epithelial functions that include secretion (12–15, 29, 30), we tested whether HTS affects Ca^{2+} homeostasis in PE and NPE cells. Analysis of fluorescent signals from cells loaded with the Ca^{2+} indicator dye Fura-2 AM showed cell swelling to be associated with significant elevations in $[Ca^{2+}]_i$ (Fig. 2 *E* and *F*). Interestingly, this effect was confined to NPE cells, in which exposure to 190 mOsm saline increased the average 340/380 ratio by 65.55 ± 7.56% from the baseline of 0.13 ± 0.021 ($n = 57$; $P < 0.0001$) (Fig. 2*F*). During continued HTS, $[Ca^{2+}]_{NPE}$ levels returned to a sustained plateau that mirrored RVD dynamics observed during volume measurements (Fig. 2 *A* and *E*, arrowheads). HTS-evoked $[Ca^{2+}]_i$ responses were not observed in the absence of extracellular Ca^{2+} (Fig. 2*D*), indicating that that Ca^{2+} influx across the plasma membrane is required for swelling-induced Ca^{2+} homeostasis. The selective TRPV4 antagonist HC-06 reduced the amplitude of HTS-evoked $[Ca^{2+}]_i$ elevations by 82.21 ± 9.55% to 0.1486 ± 0.02 ($n = 46$; $P < 0.05$) (Fig. 2*F*). To determine whether TRPV4 is necessary for mediating the osmoresponse in the hypotonic direction, we challenged CBs from *Trpv4*$^{-/-}$ tissue with HTS. $[Ca^{2+}]_i$ levels in KO NPE cells were unaffected by the exposure to HTS ($n = 53$), demonstrating that TRPV4 mediates hypotonically evoked calcium signals in NPE. Interestingly, PE cells did not respond to HTS with $[Ca^{2+}]_i$ elevations (Fig. 2*G*). These observations indicate that NPE and PE cells exhibit fundamental differences in terms of their osmotransduction and Ca^{2+} homeostasis.

Given the fundamental difference in TRPV4 sensitivity, we asked whether NPE and PE cells differ in their response to depolarization, known to induce regenerative calcium signals in rabbit CB (31). Mouse CB cells responded to depolarization evoked by increased extracellular KCl (30 mM) with $[Ca^{2+}]_i$ elevations.

Unlike the responses evoked by GSK101 and despite the fluorescence screening by PE pigment, the amplitudes of depolarization-evoked $[Ca^{2+}]_i$ signals denoted by 340/380 ratios were comparable in NPE and PE cells, and were antagonized by nicardipine (5 μM) (Fig. 2*H* and Fig. S4). Thus, depolarization-evoked $[Ca^{2+}]_i$ responses in both epithelial layers of the CB are mediated by high-threshold L-type channels.

We next addressed the functional connection linking TRPV4-mediated Ca^{2+} signaling and cell swelling by directly recording transmembrane ion fluxes in NPE cells. These experiments were performed in the presence of carbenoxolone (100 μM) and mefloquine (10 μM) to suppress potential leakage across gap junctions and hemichannels, and/or possible ATP release (16, 32, 33). As illustrated in Fig. 2 *I*–*L*, HTS evoked reversible increases in the amplitude of the transmembrane current. HTS-induced currents had outwardly rectifying current–voltage relationship, with amplitudes of −381.8 ± 77.0 pA and 732.9 ± 124.7 pA at the holding potentials −100 mV and 100 mV, respectively ($n = 8$ cells). HTS-evoked currents were significantly attenuated by HC-06 to −185.5 ± 63.0 pA and 317.0 ± 83.7 pA at −100 mV and 100 mV, respectively ($n = 7$ cells, $P < 0.05$; Fig. 2 *K* and *L*). Thus, during the NPE swelling response, TRPV4 mediates a significant portion of the membrane conductance.

TRPV4 Activation Mediates $[Ca^{2+}]_i$ Increases in NPE, but Not PE, Cells. To directly evaluate the relationship between TRPV4 activation and $[Ca^{2+}]_i$, we stimulated CB cells with the selective agonist GSK101. Stimulation with different GSK101 concentrations established an EC_{50} of ∼33 nM (Fig. S5), comparable to the half-maximal response observed in retinal neurons and glia (20, 23). Consistent with the data obtained in HTS-stimulated cells, GSK101 (25 nM) evoked large, sustained and reversible $[Ca^{2+}]_i$ elevations in NPE cells, whereas PE cells were unresponsive (Fig. 3). Altogether, a significant 74.395 ± 8.3% increase in ΔR/R over the baseline of 0.128 ± 0.022 was measured ($n = 62$ NPE cells; $n = 4$ animals; $P < 0.005$), compared with the baseline level of 0.131 ± 0.015 in PE cells ($n = 46$ cells; $n = 4$ animals; P not significant). Demonstrating specificity, agonist-induced responses in NPE were blocked by HC-06 (10 μM) ($P < 0.005$) and were not detectable in *Trpv4*$^{-/-}$ cells (Fig. 3*B*). The antagonist had an IC_{50} of ∼900 nM (Fig. S5). These data confirm that TRPV4 is functionally localized to NPE, but not PE, cells of the CB. The blockade of HTS-induced $[Ca^{2+}]_i$ elevations by HC-06 demonstrates that the channel represents a primary transducer of NPE cell swelling.

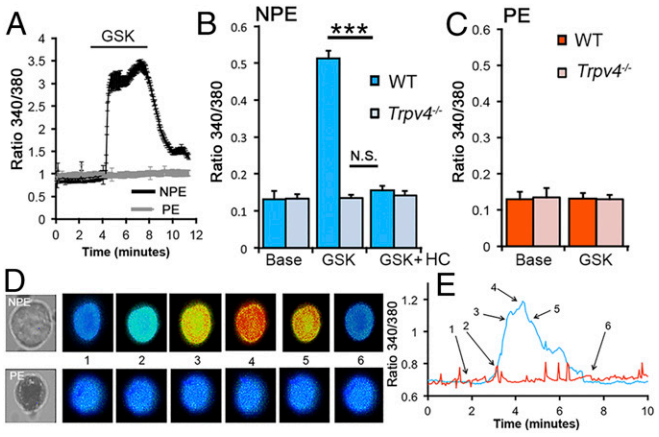

Fig. 3. TRPV4 is functionally expressed in NPE, but not PE, cells. (*A*–*C*) Dissociated cells. (*A*) The selective agonist GSK101 (25 nM) evokes $[Ca^{2+}]_i$ signals in NPE (black trace; $n = 15$), but not PE (gray trace; $n = 14$), cells. (*B*) NPE cells. GSK101-evoked responses were observed in WT ($n = 62$) but not *Trpv4*$^{-/-}$ cells ($n = 41$) and were antagonized by the selective blocker HC-06 (1 μM). (*C*) PE cells were unresponsive to GSK101 (WT, $n = 54$; KO, $n = 34$). (*D* and *E*) Representative time course of the calcium response in dissociated NPE (*Top*) and PE cell (*Bottom*) stimulated with GSK101. Note the melanin pigment in the PE cell. The timing of each calcium response in *D* is shown on the intensity time course in *E* (blue, NPE; red, PE). ***$P < 0.005$.

TRPV4 Signaling in NPE Cells Requires Activation of the Canonical Lipid Messenger Pathway. Cell swelling in numerous cell types activates the cytosolic isoforms of PLA2 (cPLA2), which is required for TRPV4 activation in some, but not all, cell types (10, 20, 23). According to a prevailing schema (20, 34, 35), the primary PLA2 product arachidonic acid (AA), a long-chain polyunsaturated ω6 fatty acid metabolite, is the precursor for epoxyeicosatrienoic acids (EETs), which function as endogenous final activators of TRPV4. To simulate this transduction pathway, we exposed CB cells to AA (50 μM). AA elevated $[Ca^{2+}]_i$ in NPE cells but had no effect on $[Ca^{2+}]_i$ levels in PE cells ($P < 0.01$) (Fig. 4*A*) and was markedly curtailed in KO NPE (Fig. S6). HC-06 inhibited AA-evoked $[Ca^{2+}]_i$ elevations in NPE cells ($n = 35$; $P = 0.023$), indicating that AA was stimulating Ca^{2+} increases primarily through TRPV4.

To test whether this pathway is activated by osmotic stress, we challenged NPE cells with HTS in the presence of the PLA2 blocker 4-bromophenacyl bromide (pBPB; 100 μM). In the presence of pBPB, HTS-evoked $[Ca^{2+}]_i$ elevations in NPE cells were blocked ($n = 29$; $P < 0.01$; Fig. 4*B*). We also observed that pBPB does not affect GSK101-evoked $[Ca^{2+}]_i$ responses ($n = 23$) ($P > 0.05$), suggesting that, as reported for HEK 293 cells heterologously overexpressing TRPV4 (35), cell swelling and agonists activate NPE TRPV4 channels through different transduction pathways. Further consistent with this canonical pathway, the eicosanoid 11,12-EET (5 μM) induced $[Ca^{2+}]_i$ increases (ΔR/R = 0.52 ± 0.076) that were also inhibited by HC-06 (ΔR/R = 0.26 ± 0.035) (Fig. 4*C*). AA- and 11′,12′-EET-evoked $[Ca^{2+}]_i$ increases were reduced or absent in *Trpv4*$^{-/-}$ NPE cells (Fig. S6). We conclude that TRPV4 activation in NPE cells involves the requisite PLA2-CYP450 step, whereas swelling does not stimulate arachidonic acid metabolism in PE cells.

It has been suggested that TRPV4 channels in anterior eye tissues such as the CB and/or trabecular meshwork might regulate IOP (18, 36). Specifically, if TRPV4 channels control the "inflow" pathway by regulating steady-state release of aqueous fluid then activation, suppression, or ablation of the channel might be expected to affect steady-state IOP. However, intravitreal injection of the antagonist (HC-06, 10 μM) or the agonist (GSK101; 75 nM) had no effect on IOP levels in WT or KO tissue (Fig. S7). Moreover, IOP levels in WT eyes were comparable to those in KOs. This suggests that TRPV4 channels are not likely to control steady-state IOP levels in healthy mouse eyes.

Discussion

We report that the polymodal TRPV4 channel is essential for osmoregulation and Ca^{2+} homeostasis in the mammalian CB. Our findings include (*i*) identification of the NPE osmosensor as TRPV4, (*ii*) discovery that calcium ions potentiate NPE swelling, (*iii*) observation of differential osmoregulation and Ca^{2+} homeostasis mechanisms in NPE vs. PE cells, and (*iv*) previously unidentified role for lipid metabolism in calcium signaling and osmoregulation within the CB. By showing differential contributions to volume regulation and Ca^{2+} signaling in a tightly coupled epithelial syncytium that plays an essential function in mammalian vision, these findings expand the known key role for TRPV4 in epithelial gene expression, intracellular signaling, protein transport, and secretion (11, 13–15, 30, 37, 38) and place it within the context of ocular volume regulation (39).

The expression of the TRPV4 gene and protein in CB was determined with transcript analyses and immunostaining and confirmed with functional studies that included excitation mapping,

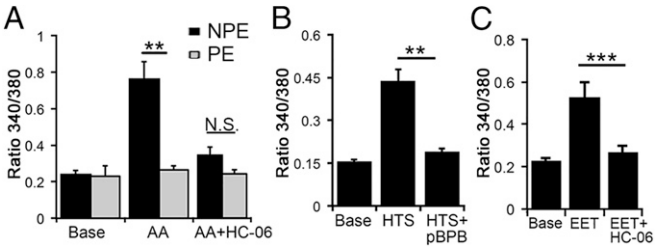

Fig. 4. TRPV4 activation in NPE cells requires activation of the canonical PLA2 pathway. Dissociated cells. (*A*) AA-evoked $[Ca^{2+}]_i$ elevations in NPE cells ($n = 30$) were antagonized by HC-06. AA had little effect on $[Ca^{2+}]_{PE}$ levels ($n = 28$). (*B*) NPE cells. The PLA2 antagonist pBPB inhibits HTS-evoked $[Ca^{2+}]_i$ signals ($n = 25$). (*C*) NPE cells. 11′,12′-EET induces $[Ca^{2+}]_i$ elevations that are antagonized by HC-06 ($n = 32$).

electrophysiology, and optical imaging in dissociated cells, ex vivo tissue, and intact mouse eyes. MRI imaging provided in vivo confirmation that TRPV4 activation induces cation influx into the CB. Antibody staining and functional analyses showed no obvious spatiotemporal differences in TRPV4 distribution, suggesting that CB regions, which vary in morphology and function (40, 41), universally use the channel to regulate their response to osmotic stress. To our knowledge, few if any studies have concurrently investigated Ca^{2+} signaling mechanisms in NPE and PE cells. Excitation mapping showed that TRPV4-induced cation influx takes place in the NPE layer but is absent from the PE layer. This is consistent with critical importance of calcium homeostasis and volume regulation in these aqueous fluid-producing cells (2, 4, 5, 32, 33, 37, 41–44). The confinement of the agmatine signal to the vicinity of the plasma membrane suggests that potent local cation clearance mechanisms (Na/K ATPases and PMCAs) limit the diffusion of Ca^{2+} signals and their spread across the NPE–PE syncytium. The absence of HTS-induced signals in Ca^{2+}-free saline, in cells with deleted *Trpv4* gene, and the effectiveness of pharmacological TRPV4 blockers suggest that TRPV4 is obligatory for transducing increases in NPE cell volume into elevated $[Ca^{2+}]_i$. Swelling-induced TRPV4-mediated $[Ca^{2+}]_{NPE}$ responses were sustained, indicating continuous activation of PLA2 (20, 34). It remains to be determined whether TRPV4-mediated Ca^{2+} signaling in NPE is modulated by downstream Ca^{2+}/calmodulin binding and/or heteromerization with other TRP subunits (e.g., refs. 21, 22, and 45).

Recent investigations have shown that TRPV4 is ubiquitously expressed in secretory and absorptive epithelia, where it regulates Ca^{2+} signaling, volume changes, cytoskeletal remodeling, and responses to shear flow and mechanical stress (11–15, 29, 39). We hypothesize that the channel influences the transepithelial CB resistance, NPE volume regulation, and fluid secretion through Ca^{2+}-dependent modulation of Na/K ATPases, PMCAs, Cl^- channels, aquaporin channels, and/or ATP release (23, 29, 32, 33, 37, 43). Multiple lines of evidence indicate that TRPV4 signaling in NPE cells requires activation of the PLA2 pathway. Thus, HTS-evoked $[Ca^{2+}]_{NPE}$ increases were inhibited by PLA2 and CYP450 antagonists. Furthermore, AA and 11,12-EET, two endogenous activators of the channel, evoked $[Ca^{2+}]_i$ elevations that were suppressed by TRPV4 blockers and channel ablation. While modulation of TRPV4 resulted in significant changes in NPE cell volume and $[Ca^{2+}]_i$ it had very little effect on PE cells. $[Ca^{2+}]_i$ signals, induced by relatively low AA concentrations (50 μM), were inhibited by HC-06, indicating that this abundant polyunsaturated fatty acid, often present in phospholipids, selectively stimulated TRPV4. Higher concentrations (>100 μM) of AA may modulate additional intracellular signaling mechanisms (possibly including Orai/ARC, Cl^-, and/or TREK1 channels) (46). If Ca^{2+} influx through TRPV4 stimulates the cPLA2 C2 domain when the enzyme is phosphorylated at serine-505, it would activate a positive feedback loop mediated through CYP450 (34, 35) whereas Ca/CaM could contribute an inactivation component through the C terminus (45).

Sensing and regulation of cell volume is of critical importance for CB cells, which continuously sustain the inflow pathway. It is therefore noteworthy that NPE and PE layers differ in volume sensing, regulation, and the expression and function of volume-activated Cl^- channels, K^+ channels, PMCAs, Na/K ATPases, and NKCC transporters (5, 33, 43, 44). The distinctiveness of volume regulatory and Ca^{2+} homeostatic apparati is consistent with the strikingly different functions in generation and secretion of aqueous humor (2, 4). Interestingly, we found that NPE and PE cells both respond to depolarization almost exclusively through high-threshold L-type voltage-gated channels. It is likely that volume-sensitive TRPV4-mediated Ca^{2+} elevations in these cells modulate Ca^{2+}-dependent Cl^- and K^+ channels (38), Ca^{2+}-CaM kinase II, volume-sensitive Cl^- currents, and/or AQP-mediated water transport (23, 32, 37, 38) that modulate RVD (23, 37), exocytosis (18), and/or secretion (32). Expression of transcripts encoding other vanilloid TRP isoforms suggests additional homeostatic complexity that might involve TRPV1-3 and TRPV6 isoforms together with metabotropic mechanisms associated with muscarinic AcH, α_2-norepinephrine, somatostatin, endothelin, bradykinin, and P2Y1/P2Y2 receptor activation (2, 4, 47–49) within NPE/PE layers and stroma.

In summary, we present evidence that links swelling-induced Ca^{2+} signals in CB NPE cells to an identified molecular channel, TRPV4. Given that Ca^{2+} regulates epithelial secretory activity (15, 30), might regulate ATP release from NPE (as shown for lens and airway epithelia; refs. 29, 39, and 47) and modulate secretion of ions, water transport, pigment production, and release of nitric oxide (18, 23, 24, 43, 48), it is not inconceivable that volume-sensitive, PLA2-dependent TRPV4 signals affect Ca^{2+}-dependent activity of Na/K ATPases, the primary determinant of aqueous humor secretion (2, 5, 32, 39). Consistent with this conjecture, topical application of Ca^{2+} ionophores elevates IOP without significantly changing the outflow facility (50). Our finding that genetic ablation and intraocular injection of GSK101/HC-06 have no effect on IOP argues against a role for the channel in steady-state maintenance of IOP (e.g., ref. 36). However, its possible sensitivity to mechanical stimuli (10, 35) suggests that TRPV4 might be overactivated during ocular hypertension. Mutations in a CB CYP450 isoform (CYP1B1) represent the predominant cause of primary congenital glaucoma (2), suggestive of possible links between elevated IOP, anomalous aqueous secretion, and biosynthesis of eicosanoid TRPV4 activators. The differential localization and function of the volume-sensitive TRPV4 channel suggests a new complexity in volume regulation of cell types forming epithelial syncytia.

Materials and Methods

Animals. Pigmented C57BL/6J, nonpigmented B6.Cg-Tg(Thy1-YFP)HJrs/J and pan-null *Trpv4*$^{-/-}$ mice with excised transmembrane domains 5 and 6 encoded by exon 12 of the TRPV4 gene (17) were maintained in a 12-h light/dark cycle with free access to food and water. *Trpv4*$^{-/-}$ mice were back-crossed with C57BL/6J mice for 10 generations so that C57BL/6J animals could be used as controls. The experiments adhered to the NIH *Guide for the Care and Use of Laboratory Animals* (51) and the ARVO Statement for the Use of Animals in Ophthalmic and Vision Research and were approved by the Institutional Animal Care and Use Committees at the University of Utah.

CB Preparation. More detail is available in *Supporting Information*. CB tissue was dissected out of the eye and plated onto Con A-coated coverslips. The NPE layer was distinguished from the PE layer by absence of melanin, DAPI staining, and outward location in the tissue. Cells were dissociated from CB in papain using published protocols (19, 20, 52) and identified based on size and melanin content (Fig. S2).

Immunofluorescence. Antibody staining in WT and KO tissue was conducted as described preciously (19, 53, 55) using rabbit anti-TRPV4 and anti-agmatine antibodies.

Superfusion of CB Tissue and Cell Swelling Assay. Changes in cell volume were measured following the Fura-2-based protocol (23, 53).

Calcium imaging was conducted following routine protocols (20, 52, 54, 55). $[Ca^{2+}]_i$ was detected using the ratiometric protocol based on the fluorescent dye Fura-2. In each experiment, ΔR/R (peak F_{340}/F_{380} ratio – baseline/baseline) quantification was obtained for multiple cells in the same visual field. Results represent cell responses from at least three animals, averaged across multiple cells and several slides per eye.

Electrophysiology. Whole-cell transmembrane currents in NPE cells were performed using standard whole-cell recording (20, 23, 54). Data acquired were sampled at 10 kHz and filtered at 2 kHz.

High-Resolution MRI. The general MEMRI procedure in mice has been described previously (25–27). For GSK or vehicle injection, 2 μL of either 100 μM GSK101 or vehicle was injected into the anterior chamber over 45 s.

Statistical Analysis. Means are shown ± SEM. Unless specified, an unpaired *t* test was used to compare two means and an ANOVA along with Tukey's multiple comparisons test was used to compare three or more means.

ACKNOWLEDGMENTS. We thank Drs. Wolfgang Liedtke (Duke University) for *Trpv4*$^{-/-}$ mice, Ning Tian for *albino* mice, and Daniel Ryskamp (University of Texas Southwestern Medical Center) for help with the initial experiments. This work was supported by the University of Utah Undergraduate Research Opportunity Program (A.O.J.); National Institutes of Health Grants EY021619 (to B.A.B.), EY022076, and P30EY014800 (to D.K.); Department of Defense Grant W81XWH-12-1-0244; Willard L. Foundation; State of Utah Technology Commercialization and Innovation Program; the University of Utah Neuroscience Initiative; and unrestricted support from Research to Prevent Blindness to Moran Eye Institute and the Kresge Eye Institute.

1. Alm A, Bill A (1973) Ocular and optic nerve blood flow at normal and increased intraocular pressures in monkeys (Macaca irus): A study with radioactively labelled microspheres including flow determinations in brain and some other tissues. *Exp Eye Res* 15(1):15–29.
2. Coca-Prados M, Escribano J (2007) New perspectives in aqueous humor secretion and in glaucoma: The ciliary body as a multifunctional neuroendocrine gland. *Prog Retin Eye Res* 26(3):239–262.
3. McLaughlin CW, Zellhuber-McMillan S, Macknight AD, Civan MM (2007) Electron microprobe analysis of rabbit ciliary epithelium indicates enhanced secretion posteriorly and enhanced absorption anteriorly. *Am J Physiol Cell Physiol* 293(5):C1455–C1466.
4. Delamere NA (2005) Ciliary body and ciliary epithelium. *Adv Organ Biol* 10:127–148.
5. Farahbakhsh NA, Fain GL (1987) Volume regulation of non-pigmented cells from ciliary epithelium. *Invest Ophthalmol Vis Sci* 28(6):934–944.
6. Miglior S, Bertuzzi F (2013) Relationship between intraocular pressure and glaucoma onset and progression. *Curr Opin Pharmacol* 13(1):32–35.
7. Woodward DF, Gil DW (2004) The inflow and outflow of anti-glaucoma drugs. *Trends Pharmacol Sci* 25(5):238–241.
8. Strotmann R, Harteneck C, Nunnenmacher K, Schultz G, Plant TD (2000) OTRPC4, a nonselective cation channel that confers sensitivity to extracellular osmolarity. *Nat Cell Biol* 2(10):695–702.
9. Watanabe H, et al. (2002) Activation of TRPV4 channels (hVRL-2/mTRP12) by phorbol derivatives. *J Biol Chem* 277(16):13569–13577.
10. Loukin S, Zhou X, Su Z, Saimi Y, Kung C (2010) Wild-type and brachyolmia-causing mutant TRPV4 channels respond directly to stretch force. *J Biol Chem* 285(35):27176–27181.
11. Harteneck C, Reiter B (2007) TRP channels activated by extracellular hypo-osmoticity in epithelia. *Biochem Soc Trans* 35(Pt 1):91–95.
12. Sokabe T, Fukumi-Tominaga T, Yonemura S, Mizuno A, Tominaga M (2010) The TRPV4 channel contributes to intercellular junction formation in keratinocytes. *J Biol Chem* 285(24):18749–18758.
13. Andrade YN, et al. (2005) TRPV4 channel is involved in the coupling of fluid viscosity changes to epithelial ciliary activity. *J Cell Biol* 168(6):869–874.
14. Mamenko M, Zaika O, Boukelmoune N, O'Neil RG, Pochynyuk O (2015) Deciphering physiological role of the mechanosensitive TRPV4 channel in the distal nephron. *Am J Physiol Renal Physiol* 308(4):F275–F286.
15. Narita K, Sasamoto S, Koizumi S, Okazaki S, Nakamura H, Inoue T, Takeda S (2015) TRPV4 regulates the integrity of the blood-cerebrospinal fluid barrier and modulates transepithelial protein transport. *FASEB J* 29(6):2247–2259.
16. Jo A, Ryskamp DA, Frye AN, Berkowitz BA, Krizaj D (2015) TRPV4 channels regulate the inflow pathway in the anterior eye. *Invest Ophthalmol Vis Sci* 56:1298.
17. Liedtke W, Friedman JM (2003) Abnormal osmotic regulation in trpv4-/- mice. *Proc Natl Acad Sci USA* 100(23):13698–13703.
18. Alkozi HA, Pintor J (2015) TRPV4 activation triggers the release of melatonin from human non-pigmented ciliary epithelial cells. *Exp Eye Res* 136:34–37.
19. Ryskamp DA, et al. (2011) The polymodal ion channel transient receptor potential vanilloid 4 modulates calcium flux, spiking rate, and apoptosis of mouse retinal ganglion cells. *J Neurosci* 31(19):7089–7101.
20. Ryskamp DA, et al. (2014) Swelling and eicosanoid metabolites differentially gate TRPV4 channels in retinal neurons and glia. *J Neurosci* 34(47):15689–15700.
21. Schaefer M (2005) Homo- and heteromeric assembly of TRP channel subunits. *Pflugers Arch* 451(1):35–42.
22. Ma X, et al. (2010) Functional role of vanilloid transient receptor potential 4-canonical transient receptor potential 1 complex in flow-induced Ca2+ influx. *Arterioscler Thromb Vasc Biol* 30(4):851–858.
23. Jo AO, et al. (2015) TRPV4 and AQP4 channels synergistically regulate cell volume and calcium homeostasis in retinal Müller glia. *J Neurosci* 35(39):13525–13537.
24. Marc RE (1999) Mapping glutamatergic drive in the vertebrate retina with a channel-permeant organic cation. *J Comp Neurol* 407(1):47–64.
25. Berkowitz BA, et al. (2009) Quantitative mapping of ion channel regulation by visual cycle activity in rodent photoreceptors in vivo. *Invest Ophthalmol Vis Sci* 50(4):1880–1885.
26. Berkowitz BA, Grady EM, Roberts R (2014) Confirming a prediction of the calcium hypothesis of photoreceptor aging in mice. *Neurobiol Aging* 35(8):1883–1891.
27. Calkins DJ, Horner PJ, Roberts R, Gradianu M, Berkowitz BA (2008) Manganese-enhanced MRI of the DBA/2J mouse model of hereditary glaucoma. *Invest Ophthalmol Vis Sci* 49(11):5083–5088.
28. Ramos de Carvalho JE, Verbraak FD, Aalders MC, van Noorden CJ, Schlingemann RO (2014) Recent advances in ophthalmic molecular imaging. *Surv Ophthalmol* 59(4):393–413.
29. Seminario-Vidal L, et al. (2011) Rho signaling regulates pannexin 1-mediated ATP release from airway epithelia. *J Biol Chem* 286(30):26277–26286.
30. Ashby MC, Tepikin AV (2002) Polarized calcium and calmodulin signaling in secretory epithelia. *Physiol Rev* 82(3):701–734.
31. Farahbakhsh NA, Cilluffo MC, Chronis C, Fain GL (1994) Dihydropyridine-sensitive Ca^{2+} spikes and Ca^{2+} currents in rabbit ciliary body epithelial cells. *Exp Eye Res* 58(2):197–205.
32. Mito T, Delamere NA, Coca-Prados M (1993) Calcium-dependent regulation of cation transport in cultured human nonpigmented ciliary epithelial cells. *Am J Physiol* 264(3 Pt 1): C519–C526.
33. Yantorno RE, Carré DA, Coca-Prados M, Krupin T, Civan MM (1992) Whole cell patch clamping of ciliary epithelial cells during anisosmotic swelling. *Am J Physiol* 262(2 Pt 1):C501–C509.
34. Watanabe H, et al. (2003) Anandamide and arachidonic acid use epoxyeicosatrienoic acids to activate TRPV4 channels. *Nature* 424(6947):434–438.
35. Vriens J, et al. (2004) Cell swelling, heat, and chemical agonists use distinct pathways for the activation of the cation channel TRPV4. *Proc Natl Acad Sci USA* 101(1):396–401.
36. Luo N, et al. (2014) Primary cilia signaling mediates intraocular pressure sensation. *Proc Natl Acad Sci USA* 111(35):12871–12876.
37. Botchkin LM, Matthews G (1995) Swelling activates chloride current and increases internal calcium in nonpigmented epithelial cells from the rabbit ciliary body. *J Cell Physiol* 164(2):286–294.
38. Shahidullah M, Mandal A, Delamere NA (2012) TRPV4 in porcine lens epithelium regulates hemichannel-mediated ATP release and Na-K-ATPase activity. *Am J Physiol Cell Physiol* 302(12):C1751–C1761.
39. Krizaj D, et al. (2014) From mechanosensitivity to inflammatory responses: new players in the pathology of glaucoma. *Curr Eye Res* 39:105–119.
40. Hara K, Lütjen-Drecoll E, Prestele H, Rohen JW (1977) Structural differences between regions of the ciliary body in primates. *Invest Ophthalmol Vis Sci* 16(10):912–924.
41. Ghosh S, Freitag AC, Martin-Vasallo P, Coca-Prados M (1990) Cellular distribution and differential gene expression of the three alpha subunit isoforms of the Na,K-ATPase in the ocular ciliary epithelium. *J Biol Chem* 265(5):2935–2940.
42. Jacob TJ, Civan MM (1996) Role of ion channels in aqueous humor formation. *Am J Physiol* 271(3 Pt 1):C703–C720.
43. Civan MM, Coca-Prados M, Peterson-Yantorno K (1994) Pathways signaling the regulatory volume decrease of cultured nonpigmented ciliary epithelial cells. *Invest Ophthalmol Vis Sci* 35(6):2876–2886.
44. Zhang JJ, Jacob TJ (1997) Three different Cl- channels in the bovine ciliary epithelium activated by hypotonic stress. *J Physiol* 499(Pt 2):379–389.
45. Watanabe H, et al. (2003) Modulation of TRPV4 gating by intra- and extracellular Ca^{2+}. *Cell Calcium* 33(5-6):489–495.
46. Meves H (2008) Arachidonic acid and ion channels: An update. *Br J Pharmacol* 155(1):4–16.
47. Farahbakhsh NA (2003) Purinergic signaling in the rabbit ciliary body epithelium. *J Exp Zoolog A Comp Exp Biol* 300(1):14–24.
48. Sharif NA, et al. (2014) Human non-pigmented ciliary epithelium bradykinin B2-receptors: Receptor localization, pharmacological characterization of intracellular $Ca^{(2+)}$ mobilization, and prostaglandin secretion. *Curr Eye Res* 39(4):378–389.
49. Martin-Gil A, et al. (2012) Silencing of P2Y(2) receptors reduces intraocular pressure in New Zealand rabbits. *Br J Pharmacol* 165(4b):1163–1172.
50. Podos SM (1976) The effect of cation ionophores on intraocular pressure. *Invest Ophthalmol* 15(10):851–854.
51. National Research Council (2011) *Guide for the Care and Use of Laboratory Animals* (National Academies, Washington, DC), 8th Ed.
52. Szikra T, et al. (2009) Calcium homeostasis and cone signaling are regulated by interactions between calcium stores and plasma membrane ion channels. *PLoS One* 4(8):e6723.
53. Chiavaroli C, Bird G, Putney JW, Jr (1994) Delayed "all-or-none" activation of inositol 1,4,5-trisphosphate-dependent calcium signaling in single rat hepatocytes. *J Biol Chem* 269(41):25570–25575.
54. Molnar T, et al. (2012) Store-operated channels regulate intracellular calcium in mammalian rods. *J Physiol* 590(15):3465–3481.
55. Witkovsky P, Gábriel R, Križaj D (2008) Anatomical and neurochemical characterization of dopaminergic interplexiform processes in mouse and rat retinas. *J Comp Neurol* 510(2):158–174.